The splicing switch of SLK controls tumor progression partially *via* different associations with occludin

Ying-Qun Yang [1,2,#], Si-Rui Zhang [1,2,#], Yue Hu [1,2,#], Jie-Fu Li [1], Jia-Wen Guan[1], Wen-Jing Zhang [3], Yu Sun [3], Jing Sun[1], Yun Yang[1], Zefeng Wang [1,*], Huan-Huan Wei [1,*]

[1] CAS Key Laboratory of Computational Biology, Shanghai Institute of Nutrition and Health, Chinese Academy of Sciences, Shanghai 200031, China

[2] University of Chinese Academy of Sciences, Beijing 100049, China

[3] Institute of Cancer Stem Cell, Dalian Medical University, Dalian 116044, China

[#] These authors contributed equally to this work

*corresponding to: weihuanhuan@picb.ac.cn (H-H. Wei),

wangzefeng@picb.ac.cn (Z. Wang).

Abstract

Aberrant RNA splicing is significantly associated with tumorigenesis and cancer progression. From a pan-cancer transcriptome analysis, we discovered a critical cancer-associated splicing event at exon 13 of SLK that encodes a fragment of 31 amino acids in its coiled-coil domain. We found that alternative skipping of this exon produces a long and short isoform (SLK-L and SLK-S). The splicing is dramatically shifted towards SLK-L across thirteen common cancer types. The two SLK isoforms have distinct functions in controlling cancer development. SLK-L is essential for cancer development while SLK-S leads to cancer repression. Mechanistically, the splicing factor Rbfox2 was identified to specifically bind intron 12 of SLK and inhibit the inclusion of exon 13. Moreover, different SLK isoforms exhibited distinct affinities in binding to the tight junction protein occludin. SLK-L bounds less occludin compared with SLK-S, which may dysregulate the function of tight junctions and disrupt the structural integrity of cells. Finally, we used antisense oligonucleotides to inhibit the inclusion of SLK exon 13, resulting in significant suppression of cancer growth and migration. Collectively, this study uncovered biological consequences and underlying mechanisms for one of the most mis-spliced genes in cancer, shedding light on new cancer therapy via splicing manipulation.

Keywords: SLK, Rbfox2, Occludin, Alternative splicing, Cancer, Antisense oligo (ASO)

Introduction

Alternative splicing (AS) of pre-mRNA is a key step in the post-transcriptional regulation of gene expression. It can produce distinct splicing isoforms from a single gene, thus expanding the proteome diversity at the RNA level. In addition to the regulation by the core spliceosome [1], AS is also controlled by the cooperation of multiple regulatory *cis*-elements that recruit *trans*-acting splicing factors to affect proximal splice sites (SS) through multifarious mechanisms [1-4]. AS governs many aspects of cellular functions, hence its dysregulation was found to be closely associated with diverse human diseases including inflammatory diseases [5,6], neuropsychiatric disorders [7-9] and cancers [10-17].

Extensive alteration in AS is considered as an established pathophysiobogical hallmark of cancers [4,14,18,19]. However, studying splicing mis-regulation in cancers is quite a challenge due to the large noise, and the diverse and complicated mechanisms. To investigate the function and regulation of AS in cancers, we have previously identified a core set of AS events that are significantly altered across multiple common cancer types through analysis of transcriptome sequencing data from The Cancer Genome Atlas (TCGA) project [14,20]. Among the core set of the cancer-associated AS genes, the splicing of STE20-like serine/threonine-protein kinase (*SLK*) was discovered significantly and extensively altered across 13 types of common cancers for the first time.

SLK is a member of the five germinal center kinase families and has diverse cellular functions. It was reported to affect the migration of mouse fibroblasts by directly interacting with LIM domain-binding protein 1 (Ldb1) [21].

It also associates with the progression of epithelial to mesenchymal transition (EMT) [22]. As a protein kinase, SLK was involved in cell cycle progression by phosphorylating PLK1 and promoting G2/M phase transformation [23,24]. In addition, SLK was found to promote apoptosis by transactive p53 [25] or activating the phosphorylation of p38 mitogen-activated protein kinase (MAPK) through ASK1 [26]. In summary, *SLK* plays an important role in cellular pathways associated with cancer progression [27,28]. However, few studies report and investigate consequences and machenisms of *SLK* splicing. Therefore, uncovering the relationship between abnormal splicing of *SLK* and cancer will provide mechanistic insight into cancer-associated alternative splicing with therapeutic potential.

Results

SLK splicing is significantly and extensively altered across thirteen common types of cancer

The human *SLK* gene is located on chromosome 10 and consists of 19 exons. The SLK protein contains the N-terminal kinase catalytic domain (encoded by exons 1 to 8), an interdomain linker, and the C-terminal coiled-coil domain responsible for protein-protein interaction (encoded by exons 11 to 19). The alternative inclusion of exon 13 in *SLK* pre-mRNA produces two isoforms, the long or short isoform (SLK-L and SLK-S), which differs at a fragment of 31 amino acids in the C-terminal coiled-coil domain (Fig. 1A, left). The comparison of the protein structures predicted by Alphafold (https://alphafold.ebi.ac.uk/,[29]) demonstrates that the exon 13 encoded sequence locates in terminus of the long α-helix within the coiled-coil domain (Fig. 1A, right), suggesting the structure-function relationship. Moreover, SLK AS event is conserved in mammals (Fig. S1A), indicating a functional importance. In a previous pan-cancer investigation of global AS dysregulation [14], we found that AS of *SLK* was significantly altered across 13 common types of cancers, with the percent spliced in (PSI) significantly increased compared to that in normal samples (i.e., increased SLK-L level in cancers) (Fig. 1B). The general AS alteration of *SLK* indicated that the two isoforms may play different roles in cancers. Moreover, the mechanism of this dysregulation may play general roles across cancers.

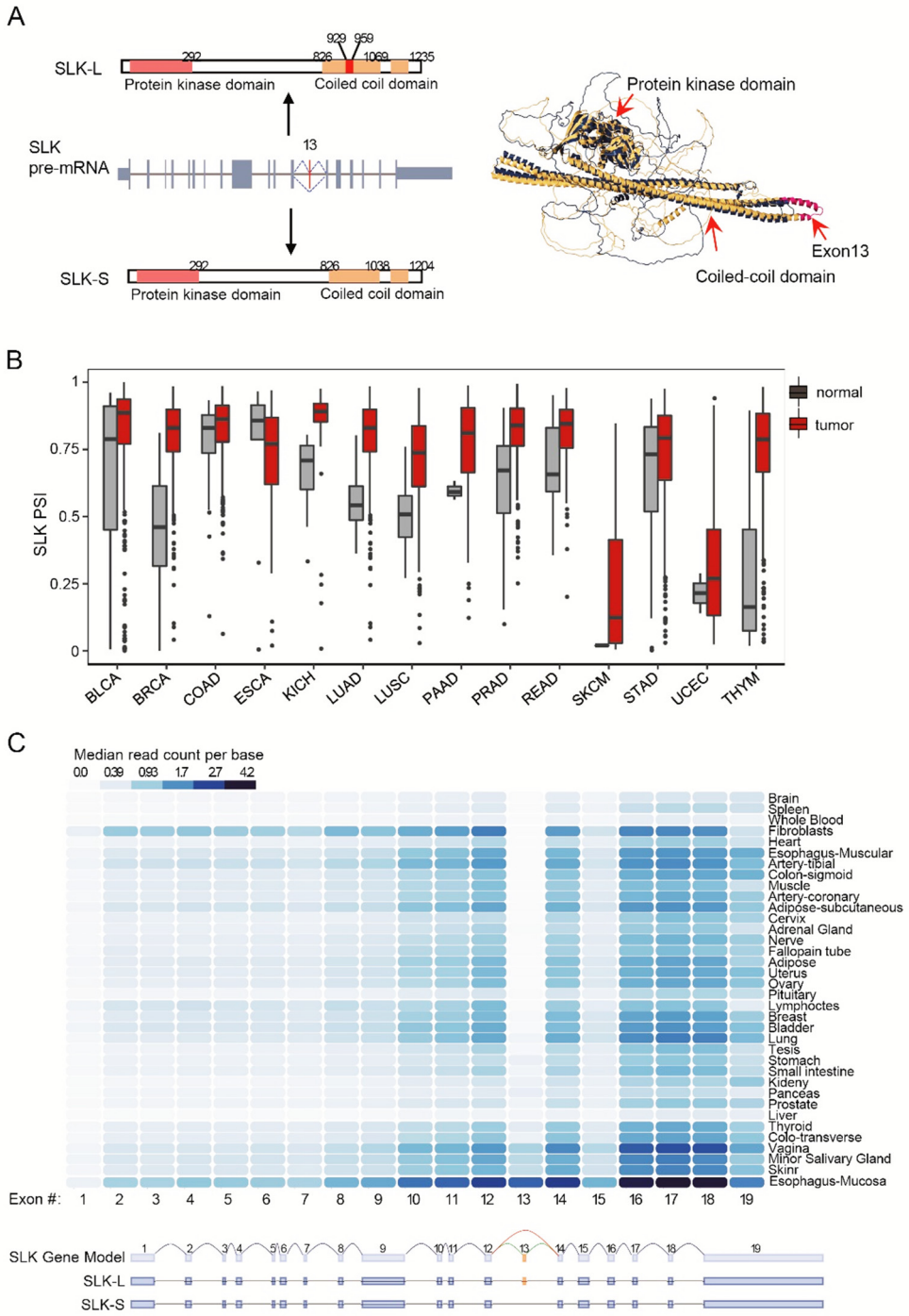

Figure 1 The alternative splicing of SLK alters dramatically in multiple types of human cancer. **A.** Left, schematics of human SLK pre-mRNA and protein. SLK-L included the 13th exon, while SLK-S skipped the 13th exon. Right, The comparison of predicted structure of SLK-L (yellow) and SLK-S isoform (blue). The alternative spliced exon 13th is highlighted in red. **B.** The SLK splicing ratios across various cancer types in TCGA database. PSI: percent spliced in. **C** The expression of SLK isoforms in multiple tissues.

We further investigated the expression of SLK isoforms in various tissues using Genotype-Tissue Expression (GTEx) data [30]. The exon count analysis showed a preference of SLK-S expression in tissues with slow self-renewal (e.g., brain), whereas the SLK-L is preferably expressed in tissues with rapid proliferation and self-renewal (e.g., skin). In particular, the non-dividing muscular tissue of esophagus mainly contains SLK-S isoform, whereas the fast renewal mucosa membrane of esophagus contains predominantly SLK-L isoform (Fig. 1C). Such pattern is largely consistent with the splicing changes of SLK in cancers that contain many actively dividing cells (Fig. 1C), implying that SLK-L may play a role in promoting cancer cell growth.

Alternative Splicing of SLK affects cancer cell progression *in vitro*

To further study the function of AS in SLK , we used siRNAs that were designed to specifically target SLK-L (binding to the 13th exon of SLK) or SLK-S (binding to the junction of the 12th and 14th exons) in colon cancer HCT116 cells (Fig. S2A-S2B). The highly invasive HCT116 cells have a normal diploid karyotype with the PSI of the SLK between 0.4-0.6, which is ideal to examine the change of AS ratio in both directions. We found that the cells with SLK-S knockdown showed normal cellular phenotypes compared to the control cells, whereas cells with SLK-L knockdown showed significant reduction in cell proliferation, anchorage-dependent colony formation, migration, and invasion (Fig. S2C-S2F), suggetsing that the two isofroms have distinct cellular functions.

To ensure the reliability and stability of these results, we used CRISPR technology to establish HCT116 stable cell lines that specifically express SLK-L or SLK-S (Fig. 2A, 2B). Consistent with the siRNA knockdown results,

HCT116 cells with only SLK-S (i.e., SLK-L depletion) showed significant reduction in cell proliferation (Fig. 2C), colony formation (Fig. 2D), cell migration (Fig. 2E), and cell invasion (Fig. 2F), again suggesting that SLK-L deficiency may suppress cancer progression. As a comparison, the cells with SLK-L only (i.e., no SLK-S) showed normal or slightly increased cell growth and cell migration (Fig. 2E-2F, Fig. S2E-S2F), suggesting that SLK-L isoform (but not SLK-S) is required for the robust proliferation and migration of cancer cells.

We further test if the observed cellular phenotypes were directly caused by the AS changes of SLK. The isoform-specifc re-expression of SLK-L and SLK-S was conducted in SLK knockout (SLK KO) HCT116 cells generated by CRISPR-cas (Fig. 3A-3B). The cells with re-expression of SLK-L showed restoration of cell proliferation and migration/invation, whereas the cells with re-expression of SLK-S were similar to the SLK-KO cells (Fig. 3C-3F), indicating that the SLK-L isoform facilitate the proliferation and migration of cancer cells.

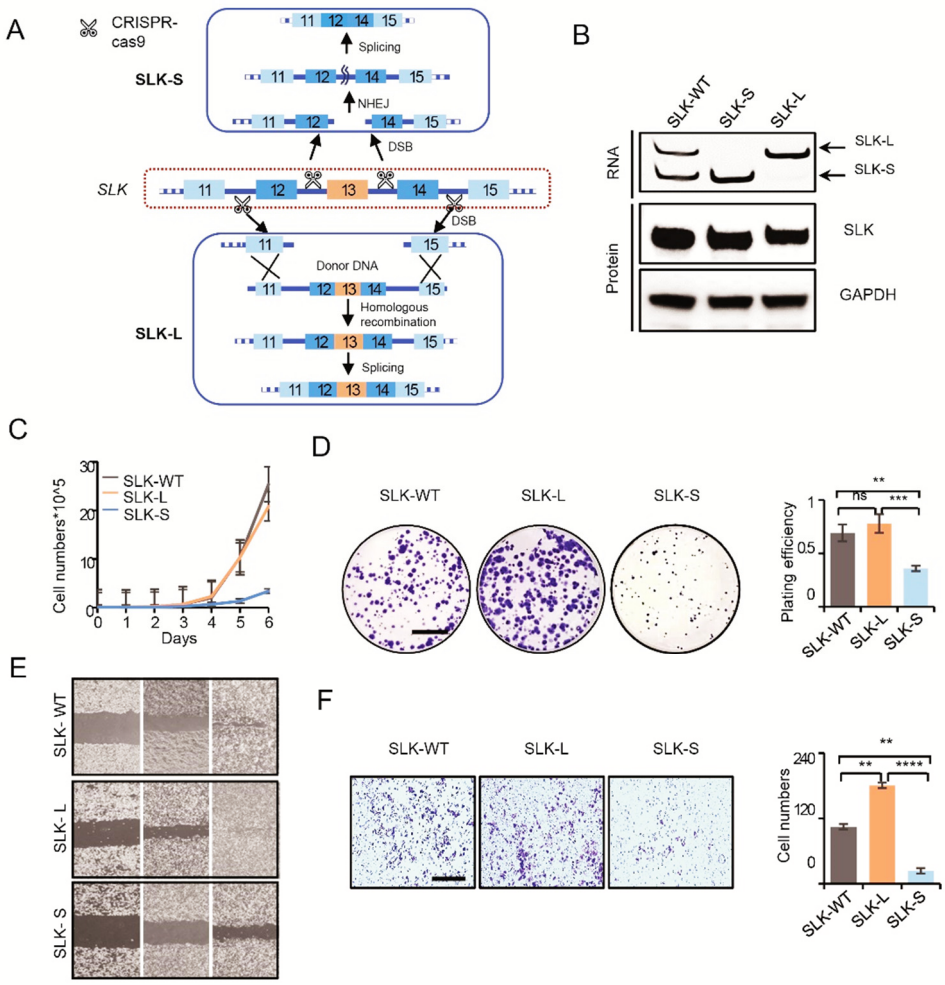

Figure 2 The cancer cells stably express SLK isoforms were generated by CRISPR-cas and exhibited different proliferation and metastasis abilities.**A.** HCT116 cells expressing different SLK isoforms were constructed by CRISPR. **B.** The RNA and protein levels of SLK under gRNA mediated CRISPR genome editing. **C-F.** Cancer cell progression was measured from triplicate experiments, with p values calculated by one-way ANOVA and Tukey's test. **C.** various SLK cells were grown for 6 days, with cell numbers counted every day (n=3) to measure cell growth **D.** anchorage-dependent colony formation of different SLK cell lines (n=3; scale bar:1 cm). The planting efficiency was quantified with ImageJ. **E.** *in vitro* migration of different SLK cell lines was analyzed by wound healing assay (n=3). **F.** cell invasion was measured by transwell assay (n=3; scale bar: 200 μm). Cell number was quantified with ImageJ. *P<0.05, **P<0.01, ***P<0.001, ****P<0.0001, ns, not significant. The chart represents mean±SD.

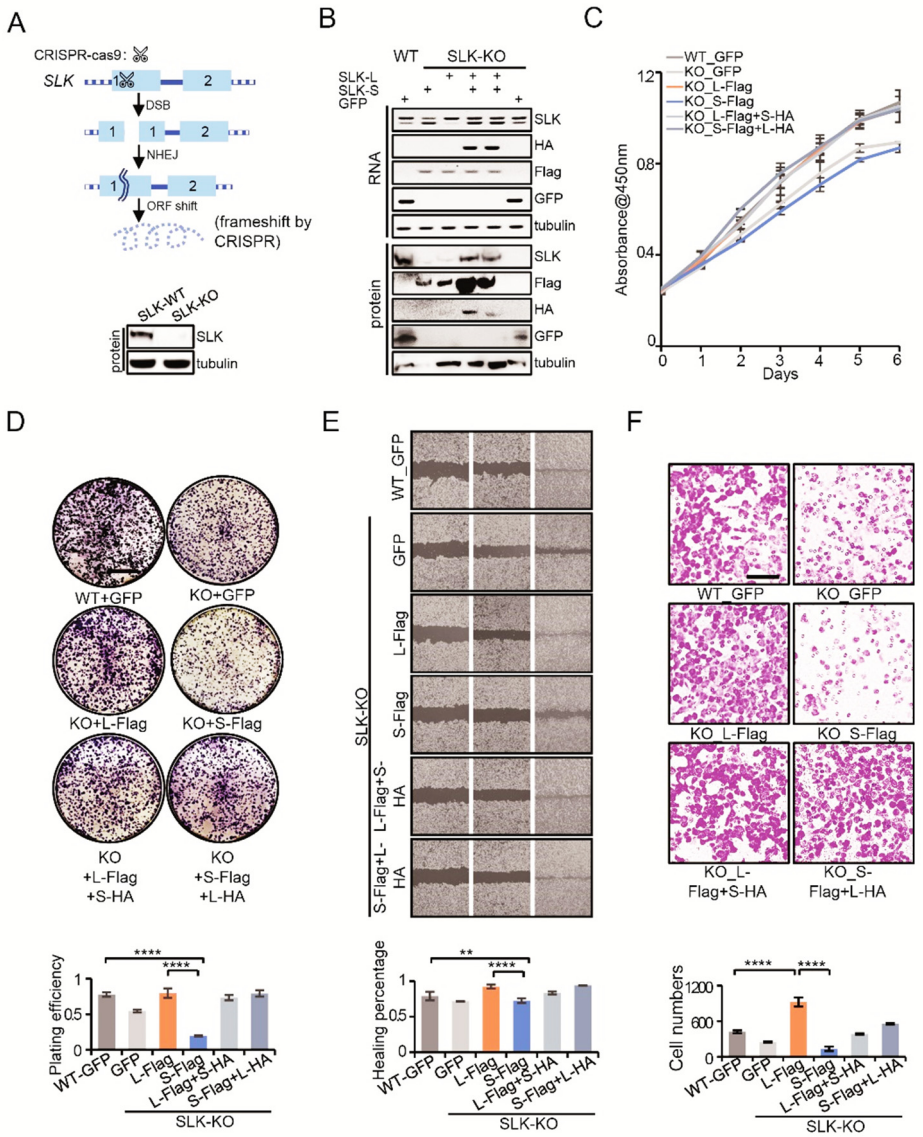

Figure 3 Cancer progression was restored by recovering the expression of the SLK isoforms.**A.** Construction of SLK knockout cell line by CRISPR. **B.** SLK isoforms were re-expressed in SLK knockout cells, with the RNA and protein level of SLK detected accordingly. **C-F.** Cancer cell development was measured as described in Fig. 2.

Alternative Splicing of SLK affects cancer cell progression *in vivo*

To examine whether dysregulation of SLK AS can affect cancer growth *in vivo*, we generated xenograft mouse model using HCT116 cells containing a single SLK isoform or with SLK knockout. We inoculated nude mice with the

four types of cells in two different dosages ($5x10^6$ cells for Fig. S3, and $1x10^6$ cells for Fig. 4), and followed the tumor growth. As expected, the size of the subcutaneous tumors increased rapidly in wild-type (WT) and SLK-L groups while they were in smaller size in the SLK-S and SLK-KO groups, especially in the SLK-S group (Fig. 4A-4B and Fig S3A-3B). In terms of the tumor weight, the SLK-S and SLK-KO groups showed significantly lower weight than the wild-type and SLK-L groups (Fig. 4C). This results indicated that the cellular proliferation was inhibited in the SLK-S/SLK-KO group which lacks SLK-L, suggesting the deficiency of SLK-L had the potential for cancer suppression.

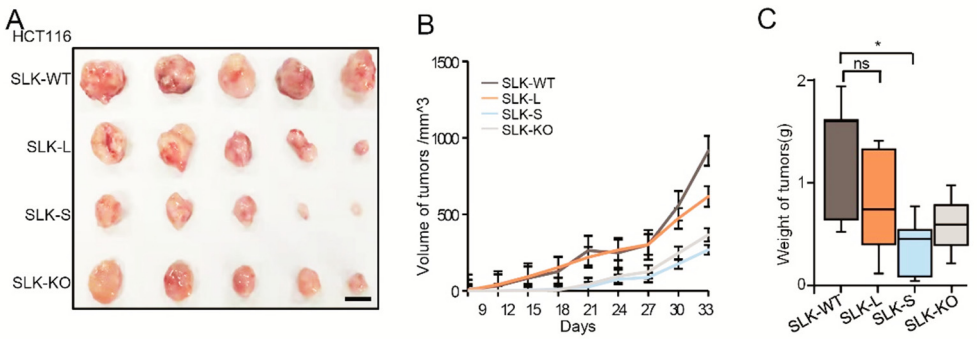

Figure 4 The deficiency of SLK long isoform inhibits tumor growth in xenograft mice. **A** Xenograft tumors were generated using nude mice injected with SLK-WT, SLK-L, SLK-S, or SLK-KO cells (1×10^6 cells/mouse), respectively. **B.** Tumors were removed after five weeks, and tumor volume was quantified (n=5). **C** The weight of xenograft tumors were plotted as box plot. The chart represents mean±SD. *P<0.05, ns, not significant. Dunnett's test was used in B and C.

Rbfox2 regulates SLK alternative splicing

Since the AS of SLK exhibited significant effects on cancer development, we aim to investigate how SLK splicing is regulated. We queried the ENCODE eCLIP dataset [31] to identify the possible splicing factors that regulate the AS

of SLK. As a result, several splicing factors were discovered to have binding peaks near the 12th intron and the 13th exon of SLK, including Rbfox2, QKI, and HNRNPA1 (Fig. 5A and S4A). To test the functions of these splicing factors, we overexpressed them, and found Rbfox2 and QKI could changed the AS of SLK while HNRNPA1 exhibited less influence (Fig. S4B). In addition, the RNA immunoprecipitation (RIP) assay confirmed the binding of Rbfox2 (not QKI) to SLK RNA (Fig. 5B). Rbfox2 is a member of the RNA-binding Fox proteins (Rbfox) family which regulates splicing by binding to the motif (5'-UGCAUGU-3') on the pre-RNAs [32-35]. The expression of Rbfox2 is found decreased in several types of cancers(Fig. 5C).

We hypothesized that Rbfox2 inhibited SLK splicing by binding to its pre-RNA. To validate this hypothesis, we checked the sequence of SLK RNA and found two Rbfox2 binding motifs in the 12th intron. Then we constructed SLK splicing reporters with the correct or mutated Rbfox2 binding motifs to assess the regulatory mechanism of Rbfox2 (Fig. 5D). We also tested splicing of the SLK reporters in cells undergoing Rbfox2 overexpression or knockdown. As expected, in Rbfox2-overexpressed cells, AS of the wild-type SLK reporter tended to skip the 13th exon, producing more SLK-S. However, the skipping ability of the mutated reporter was attenuated, leaving the splicing ratio similar to the mock control (Fig. 5E). On the contrary, the SLK-WT reporter tended to retain the 13th exon in Rbfox2 knockdown cells, resulting the AS shift towards SLK-L. Furthermore, the splicing of mutated reporters was not altered with Rbfox2 deficiency (Fig. 5F). The reporter gene assay confirmed that Rbfox2 regulates SLK alternative splicing by binding to the motif sequence 5'-

UGCAUG-3' in the 12th intron to promote the skipping of SLK exon 13th, resulting in lower PSI and decreased SLK long isoform.

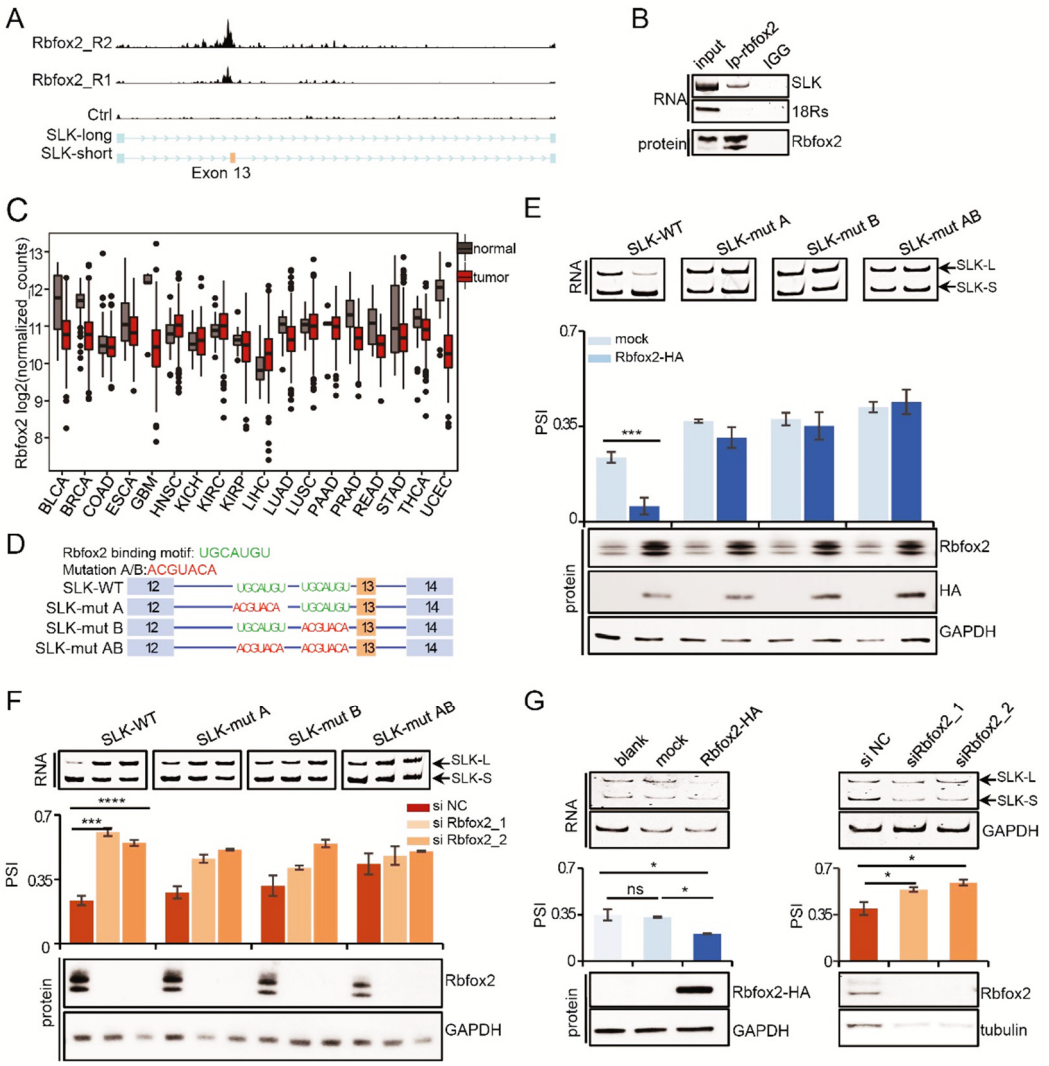

Figure 5 Rbfox2 regulates the splicing of SLK. **A.** Rbfox2 binding peaks was detected in front of the SLK exon 13th. **B.** The RIP assay showed the binding of Rbfox2 to SLK RNA. **C.** Rbfox2 expression level in tumors versus normal tissues across various cancer types from TCGA data. **D.** The minigene reporter of SLK wildtype and mutants were constructed. **E-G.** Rbfox2 regulates SLK splicing through its binding motif. **E.** Rbfox2 overexpression inhibited SLK minigene splicing. **F.** Rbfox2 knockdown promoted SLK minigene splicing. **G**. Rbfox2 regulates splicing of the endogenous *SLK* gene. RNA loading control: GAPDH; protein loading control: GAPDH or Tubulin. The chart represents mean±SD. *P<0.05, **P<0.01, ***P<0.001, ****P<0.0001. Two-way ANOVA was applied to analyze the difference among means in E and F while one-way ANOVA was used in G.

In addition, we tested the regulation of Rbfox2 to endogenous AS of SLK. Rbfox2 was either overexpressed or knocked down in cancer cells to regulate the AS. The results were consistent with that of the SLK reporter. Endogenous exon 13th of SLK skipped after overexpression of Rbfox2 as compared to nonspecific and negative controls (Fig. 5G, left), whereas it was included after knockdown of Rbfox2 by siRNA (Fig. 5G, right). Collectively, the results demonstrated that Rbfox2 can inhibit SLK AS by binding to its recognition motif on the SLK 12th intron.

SLK isoforms can influence cell functions at least partially through their different binding abilities to occludin.

We next sought to determine how different isoforms of SLK decide cancer progression. Considering that the SLK-S lacks 31 amino acids which is encoded by exon 13 and forms a short coiled-coil domain (Fig. 1A), we initially predicted that this would affect the subcellular localization of SLK isoforms. However, immunofluorescence localization assay exhibited no significant difference between SLK isoforms (Fig. S5A).

Cell function experiments revealed that the different isoforms of SLK had obvious impact on cell migration and mobility. In addition, SLK was reported to play necessary roles in the epithelial-to-mesenchymal transition (EMT) process [22,36,37] and regulate the focal adhesion turnover [38]. Therefore, we hypothesized that SLK isoforms were involved in EMT pathway. We tested the biomarker of EMT such as E-cadherin, occludin, N-cadherin, and vimentin to assess whether SLK is associated with these proteins. Interestingly, among them, occludin was detected to be differentially expressed in SLK-L versus

SLK-S stable cell lines. SLK-S has a higher expression level of occludin than SLK-L (Fig. 6A).

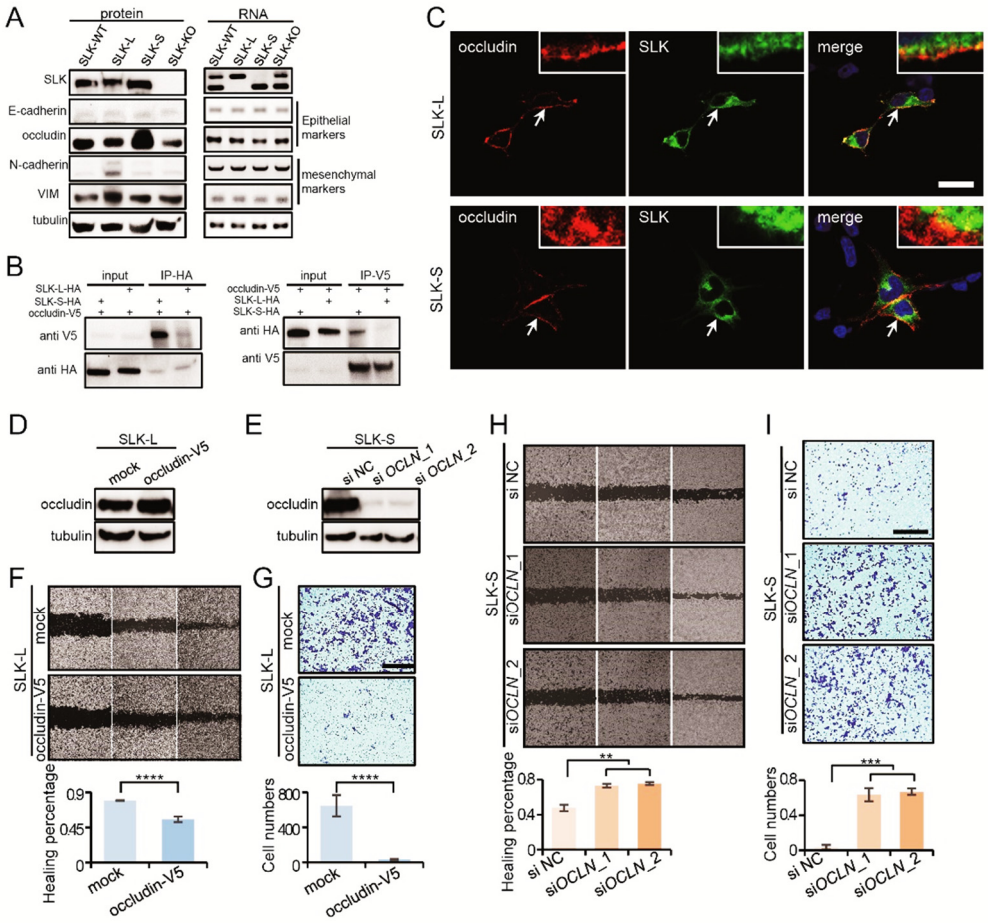

Figure 6 SLK isoforms influence cell functions partially through their different binding abilities to occludin. **A.** Selected EMT markers were tested in different SLK cell lines. **B.** SLK isoforms showed varied binding abilities with occludin. **C.** The subcellular localization of SLK and Occludin. Scale bar: 20 μm. **D-E.** Overexpression or knockdown of occlidin in SLK-L or SLK-S cells. **F-I.** Cell migration (n=3) and invasion (n=3; scale bar:200 μm) were tested as described in Fig. 2. *P<0.05, **P<0.01, ***P<0.001, ****P<0.0001.

Occludin is considered as a staple of tight junctions and performs vital functions in EMT, which contributes to cancer metastasis [39]. To address whether SLK isoforms interact differecially with occludin, we test their interaction through both immunoprecipitation and localization.

Immunoprecipitation showed that SLK isoforms had different binding capabilities with occludin. The SLK-S had a stronger binding ability to occludin, while the SLK-L was barely bound to occludin (Fig. 6B). Furthermore, the immune colocalization demonstrated that both SLK isoforms and occludin localized around the cell membrane (Fig. 6C), indicating the possible interaction between SLK and occludin. Given cancer cells with low occludin expression are more likely to migrate and invade [40], we assess the relationship between occludin expression level and cell development in this study. Consistently, the overexpression of occludin in SLK-L cells could inhibit cell migration and invasion, whereas knockdown occludin in SLK-S cells promoted cell migration and invasion (Fig. 6D-6I). These results indicated that SLK-L may work as cancer-causing proteins. The overexpessed SLK long isoform may disrupt the interaction between SLK-S and occludin, leading to the dysregulation of TJs and subsequent cell fate. Together, our studies partially explained why cells with high expression of SLK-L exhibited carcinogenicity and promote cancer progression.

ASOs affected cell functions by regulating SLK splicing

From the phenotype of SLK splcing swith in both cells and mice, we speculated that the disparity in biological functions of SLK isoforms could enable us to target SLK splicing for cancer therapy. Therefore, we attempted to manipulate the AS of SLK artificially, evaluating the feasibility of RNA-level gene therapy. Antisense oligonucleotides (ASOs) could specifically bind to the splicing site to inhibit the binding of other splicing factors, thus modifying RNA splicing [41]. We designed ASOs that pair with the splicing site of the 13th exon

of SLK to inhibit its splicing, trying to reduce the expression of SLK-L (Fig. 7A). Among the designed eight ASOs, ASO6 and ASO8 exhibited significant inhibiton to SLK splicing (Fig. 7B). Furthermore, we treated cells with ASO6 and ASO8 to evaluate the effect of the ASOs in cancer cell progression. As a result, both ASO6 and ASO8 reduced the proliferation, migration, and invasion abilities of HCT116 cells (Fig. 7C-7F). Collectively, these results showed that artificial modulation of SLK spicing by ASO has potential in cancers therapy.

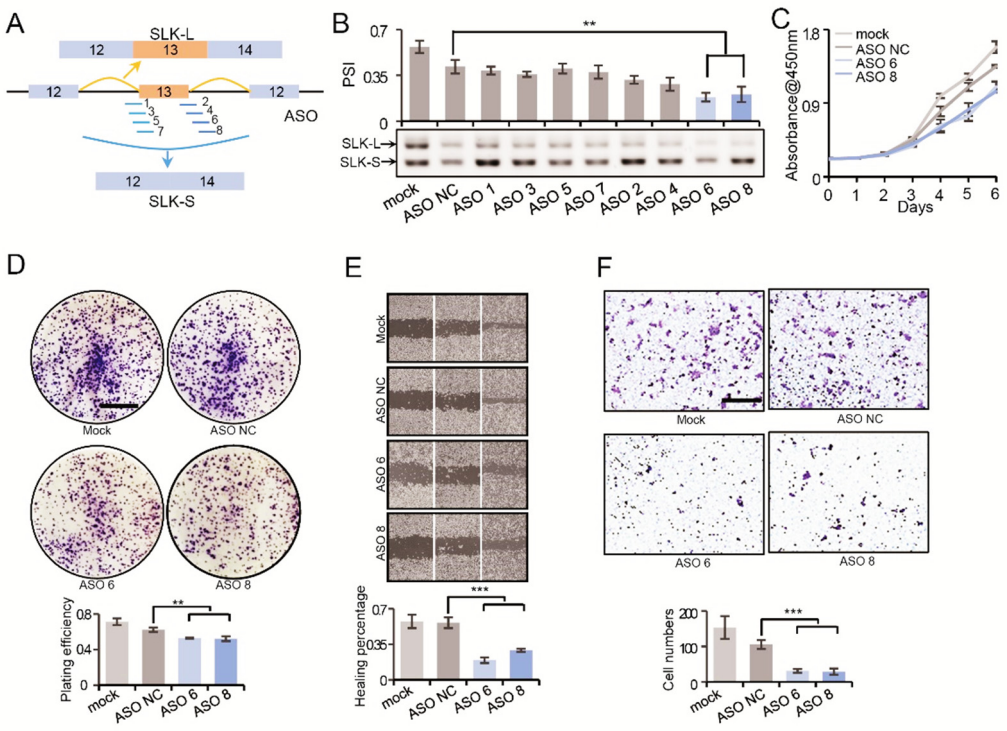

Figure 7 ASOs affected cancer progression by regulating SLK splicing. **A** The Design of ASOs that specifically block SLK splicing. **B** The PSI of SLK splicing in cells treated with indicated ASOs. **C-F** Cellular proliferation rates (C; n=3), colony formation (D; n=3; scale bar: 1 cm); migration (E; n=3), and invasion (F; n=3; scale bar: 200 μm) were tested according to Fig. 2 *P<0.05, **P<0.01, ***P<0.001, ****P<0.0001, ns, not significant.

Discussion

More than 90% of human genes undergo alternative splicing [42]. After eliminating noises caused by tissue-specific splicing, numerous gene-splicing alterations have been detected in large amount of cancer patients [14]. Abnormal splicing is considered as a molecular hallmark of cancer thus worth efforts in investigating the underlying mechanisms, the cellular consequences, and the possibility of manipulation, for the purpose of cancer treatment. In this study, we have demonstrated that the SLK splicing event is impressive and notable due to the significant and extensive alteration across 13 types of common cancer. We have discovered that the expression ratio of the two protein isoforms produced by SLK AS has distinct cellular functions, with SLK-L being crucial for cancer development. In particular, the cancer cell progression was suppressed through downregulation of SLK-L. In addition, we discovered the cells with SLK-S produced significant smaller subcutaneous tumors than other groups in tumorigenesis experiments in nude mice, which supports the hypothesis that the AS of the *SLK* gene could be used as a target for tumor therapy. Furthermore, by regulating SLK splicing via ASOs to reduce the expression of SLK-L, we have identified several ASOs that can inhibit cancer development, especially in cell metastasis such as migration and invasion. However, these need further verification in different cancer types and *in vivo*.

The mechanisms of the SLK splicing were found to be complicated. The AS of SLK was proved to be regulated by Rbfox2 through the binding motif 5'-UGCAUG-3' on SLK pre-RNA. However, though overexpression of Rbfox2 can suppress SLK exon 13 splicing, its inhibition efficiency is much less than that of

the ASOs, indicating ASOs may affect other splicing factors. Moreover, the expression of Rbfox2 was not simultaneously altered in the same cancer types compared with SLK splcing, implying the AS of SLK could be regulated in a more complicated manner. In addition, Rbfox2 was reported to form large assembly of splicing regulators (LASR) [43,44], thus the components of LASR also has potential in affecting SLK splicing.

We have discovered that occludin may have different binding abilities to different SLK isoforms, However, the precise mechanism of how they interact with each other remained further exploration. Most of occludin functions were initially attributed to conformational changes following selective phosphorylation [45], hence more solid validations between SLK AS and occludin are required.

In summary, the expression levels of SLK isoforms showed drastic variations in tumor cells and normal cells. We found that different isoforms of the *SLK* gene had different biological functions. SLK long isoform is crucial for cancer maintenance and development. Rbfox2 inhibited SLK exon 13 splicing through its binding motif. SLK isoforms might affect cell functions by the different binding abilities of occludin. The regulation of SLK splicing by using ASOs significantly changed the expression ratio of SLK isoforms and markedly inhibited cell migration and invasion. Our study offers insights into SLK splicing and provides a novel approach for cancer therapy by targeting the splicing of the *SLK* gene.

Materials and methods

Plasmid construction

The CDS sequences of SLK-L and SLK-S were amplified from the cDNA of HCT116 cells. The two SLK isoforms were cloned into the pcDNA3.1 overexpression vector with the HA or V5 tag sequence. The CDS regions of SLK isoforms and the HA or Flag tag sequence were inserted after the CMV promoter of the pCDH backbone plasmid to create lentivirus vectors. The Rbfox2 CDS region with the HA tag was cloned into the pcDNA3.1 backbone to produce Rbfox2 overexpression vectors.

For the SLK minigene reporter, we cloned SLK exon 12, 13, 14, a 337-nt sequence with 5'-SS, a 290-nt sequence containing branch point and 3'-SS of intron 12, and a partial sequence of intron 13, into the pcDNA3.1 plasmid backbone. The SLK mutation vectors were constructed by replacing the Rbfox2 binding motif 5'-TGCATGT-3' with 5'-ACGTACA-3'.

Mammalian cell culture

HEK 293T (ATCC CRL-3216) cells were cultured in Dulbecco's modified Eagle's medium with high glucose (C11995500BT, Gibco) supplemented with 10% fetal bovine serum (FBS). HCT116 (CCL-247) cells were cultured in McCoy's 5A medium (16600-082, Gibco) supplemented with 10% FBS.

Transfection

Transfection procedures were carried out according to the user instruction of Lipofectamine 3000 (L300015, Thermo Fisher Scientific).

RNA extraction and reverse transcription

Total RNAs were extracted by TRIzol. The concentrations of RNAs were measured by Nano-1000. The total RNA was reverse transcribed to cDNA using the PrimeScript RT reagent Kit with gDNA Eraser (RR047A, Takara).

Western blot

The cell media were removed, and adherent cells were washed with PBS before the addition of cell lysis buffer. Cell lysates were collected in 1.5 mL tubes and lysed on ice for 30 min. The suspension was centrifuged at 15000 rpm at 4 °C for 30 min to obtain supernatants. The supernatants were added to 5× SDS-PAGE buffer and incubated at 98 °C for 10 min. The reaction mixtures were resolved by 4–12% SDS-PAGE Gel (M41212C, GenScript), and the isolated proteins were transferred to PVDF membranes. The primary antibodies, namely anti-Rbfox2 (HPA006240, Sigma), anti-SLK (19743–1-AP, Proteintech), anti-Occludin (27260–1-AP, Proteintech), anti-HA (C29F4, CST), anti-V5 (D3H8Q, CST), anti-Flag (F1084, Sigma), anti-GAPDH (14C10, CST), and anti-Tubulin (11224–1-AP, Proteintech), anti-VIM (10366-1-AP, Proteintech), anti-E-cadherin (208741-1-AP, Proteintech), were used according to the manufacturer's instructions. The secondary antibody, HRP-linked goat anti-mouse IgG (#7076, CST) and goat anti-rabbit IgG (#7074, CST), were used at 1:2000 dilution. The protein bands were detected through enhanced chemiluminescence substrates and the ChemiDoc Touch Imaging System (Image Lab, Bio-Rad).

Co-immunoprecipitation

293T or HCT116 cells were seeded in a 15-cm dish and transfected with HA-tagged SLK isoforms and V5-tagged candidate proteins. The PBS-washed cells were used after transfection for 48 h. The lysis buffer (P0013, Beyotime)

was then add into the cells and the supernatants were collected after centrifuging at 15000 rpm at 4 °C for 30 min. Next, 10% supernatant was retained as input and the pallet was resuspended. Primary antibodies (HA-Tag Mouse mAb #2367 and V5-Tag Rabbit mAb #13202, CST) were added and incubated overnight. The antibodies were diluted at the ratio of 1:100. Subsequently, 50 μl protein A/G agarose beads were added to each tube and incubated at room temperature for 1 h. Following centrifugation at 2500 rpm for 5 min, the supernatants were removed, and the agarose beads were resuspended in 500 μl IP buffer and washed at room temperature for 3 times. After washing step, 50 μl of 2×SDS protein loading buffer was added, and the denatured proteins were obtained by incubation at 98 °C for 10 min.

RNA Immunoprecipitation

Cells grown in a 15-cm dish (90% confluence) were digested with 3 mL of 0.25% trypsin at 37 °C for 2 min. Next, 5 mL of complete medium was added to the dish to terminate digestion. The collected cells were subjected to RNA immunoprecipitation following the Abcam protocol (https://www.abcam.com/epigenetics/rna-immunoprecipitation-rip-protocol).

Cell development and function

Cell proliferation were analyzed by cell counting or CCK-8 assay. For cell counting, 5000 cells were seeded per well on 24-well plates, and the cell number was counted at 24, 48, 72, and 96 h after incubation. For CCK-8 assay, 1000 cells were seeded per well on 96-well-plates, and the Cell Counting Kit-8 (CCK-8, 40203ES60, Yeason) was used to determine the cell proliferation.

Colony formation assay was carried out to test the tumor formation ability of cancer cells. In brief, 2000 cells were seeded onto a 6-well plate in a

complete medium with 10% FBS for one week. The cells were then dyed with crystal violet for 30 min before washing with PBS. The plating efficiency was calculated using colony numbers divided by seeded cell numbers.

Cell migration ability was measured through wound healing experiments. Cells were seeded onto a 6-well plate. After reaching 90% confluence, the cells were scratched with a 200-μl pipette tip. The images were captured at 0, 12, 24, and 48hr after scratching. The average value of wound closure was quantified by Image J software. Experiments were performed in triplicates.

Transwell invasion assay was used to determine the invasion ability of cells. Matrigel Matrix (356234, Corning) was thawed at 4 °C and mixed with medium without FBS at the ratio of 1:8. Next, 50 μl of the mixture was added to each Transwell and incubated at 37 °C for 1 h. Subsequently, 1×10^5 cells (2×10^5 cells in Fig 3F) were seeded in each Transwell in 200 μl medium without FBS, and 500 μl medium with 10% FBS was added as an inducer in the 24-well-plate. The cells were cultured at 37 °C for 24 h. The matrix and media were removed, and the cells were incubated with 4% paraformaldehyde (PFA) for 30 min after washing with PBS. After removing of PFA, the cells were washed with PBS twice. The cells were then stained with crystal violet for 30 min and de-stained with PBS twice before imaging. Cells were counted from the captured images by using Image J software. Each experiment was repeated three times.

Lentivirus packaging and infection

HEK 293T cells were plated at 90% confluence in a 10-cm dish before transfection with plasmids. The envelope plasmid pMD2.G, the packaging plasmid psPAX2, and the transfer plasmids were co-transfected into HEK 293T

cells by Lipofectamine 3000. The mediums with lentivirus from transfected cells were collected after 48 h of transfection and filter through a 0.22-μm membrane.

Xenograft tumor formation

We conducted two biological replicants of tumorigenesis experiments in nude mice. In the first replicant, 5×10^6 cells were resuspended in PBS and injected subcutaneously into a BALB/c-nu mouse (10 mouse/group). The body weight and tumor volume were measured twice a week after injection. In SLK-WT and SLK-L group, several mice were sacrificed before the end point due to the fast-growing of tumors and the following tissue rupture. In the second biological replicant, 1×10^6 cells were resuspended in PBS and injected subcutaneously into a BALB/c-nu mouse. The tumor volume were measured every three days. The experiment was terminated at 33 days after injection . The tumor volume was calculated as volume (mm^3) = $L \times W^2/2$, where L is the largest diameter and W is the smallest diameter of the tumor. After the experiment, the mice were euthanized, and the tumor was dissected.

Immunofluorescence

293T cells were seeded in a Nunc™ dish (150680, Thermo) and transfected with HA-tagged SLK isoforms and V5-tagged occludin (for Fig 6C) or SLK different isoforms with HA or V5 tag (for Fig S5). Cells were incubated with 4% PFA for 1h. After washed with PBS, cells were incubated with 1mL 0.25% Triton™ X-100 (9036-19-5, Meck) per dish for 10 min. Then cells were washed with PBS twice and incubated with HA and V5 antibody (dilution ratio : 1:1000) at 4°C overnight. Alexa Fluor® 594 (ab 150080, abcam) and Alexa Fluor® 488 (ab 150077, abcam) were Incubated with cells at room temperature

for 1h. The nuclei were stained with DIPA (P36985, Invitrogen™) and observed and photographed under Zeiss LSM880.

Bioinformatic analyses

To identify the alternative splicing of SLK, we downloaded the level3 RNA-seq data from TCGA (http://gdac.broadinstitute.org/) and GTEx (http://gtexprotal.org/home/), and calculated PSI values of SLK in each sample. The processed signal files (in bigwig format) from eCLIP-seq of several RBPs were downloaded from ENCODE consortium. R package 'Gviz' and 'rtracklayer' were used to visualize the binding peaks of several RBPs. Other plots were generated using R package 'ggplot2'.

Structure prediction of SLK-L and SLK-L

We used Parafold[46], a paralyzed accelerated version of alphafold2[29], to predict the structure of SLK-L and SLK-S. The input is the RNA sequence of open reading frame of each isoform. Deepmind monomer model sets were employed for generating the prediction. The top 5 ranked results were investigated according to alphafold default evaluation.

Data Availability

eCLIP data of RBPs and the processed signal files (in bigwig format) were downloaded from ENCODE consortium (https://www.encodeproject.org). Custom computer code and original data are available upon request.

ReferenceUncategorized References

1. Matera AG, Wang Z: **A day in the life of the spliceosome.** *Nat Rev Mol Cell Biol* (2014) **15**(2):108-121.

2. Sveen A, Kilpinen S, Ruusulehto A, Lothe RA, Skotheim RI: **Aberrant rna splicing in cancer; expression changes and driver mutations of splicing factor genes.** *Oncogene* (2016) **35**(19):2413-2427.

3. Biamonti G, Catillo M, Pignataro D, Montecucco A, Ghigna C: **The alternative splicing side of cancer.** *Semin Cell Dev Biol* (2014) **32**(30-36.

4. Wang Y, Bao Y, Zhang S, Wang Z: **Splicing dysregulation in cancer: From mechanistic understanding to a new class of therapeutic targets.** *Sci China Life Sci* (2020) **63**(4):469-484.

5. Wu W, Syed F, Simpson E, Lee CC, Liu J, Chang G, Dong C, Seitz C, Eizirik DL, Mirmira RG, Liu Y *et al*: **The impact of pro-inflammatory cytokines on alternative splicing patterns in human islets.** *Diabetes* (2021).

6. Berger K, Somineni H, Prince J, Kugathasan S, Gibson G: **Altered splicing associated with the pathology of inflammatory bowel disease.** *Hum Genomics* (2021) **15**(1):47.

7. Barki M, Xue H: **Gabrb2, a key player in neuropsychiatric disorders and beyond.** *Gene* (2022) **809**(146021.

8. Latorre E, Mesonero JE, Harries LW: **Alternative splicing in serotonergic system: Implications in neuropsychiatric disorders.** *J Psychopharmacol* (2019) **33**(11):1352-1363.

9. Glatt SJ, Cohen OS, Faraone SV, Tsuang MT: **Dysfunctional gene splicing as a potential contributor to neuropsychiatric disorders.** *Am J Med Genet B Neuropsychiatr Genet* (2011) **156B**(4):382-392.

10. Coltri PP, dos Santos MGP, da Silva GHG: **Splicing and cancer: Challenges and opportunities.** *Wires Rna* (2019) **10**(3).

11. Dong X, Chen R: **Understanding aberrant rna splicing to facilitate cancer diagnosis and therapy.** *Oncogene* (2020) **39**(11):2231-2242.

12. Wang BD, Lee NH: **Aberrant rna splicing in cancer and drug resistance.** *Cancers (Basel)* (2018) **10**(11).

13. Jansen AM, van der Klift HM, Roos MA, van Eendenburg JD, Tops CM, Wijnen JT, Hes FJ, Morreau H, van Wezel T: **Rna analysis of cancer predisposing genes in formalin-fixed paraffin-embedded tissue determines aberrant splicing.** *Eur J Hum Genet* (2018) **26**(8):1143-1150.

14. Tsai YS, Dominguez D, Gomez SM, Wang Z: **Transcriptome-wide identification and study of cancer-specific splicing events across multiple tumors.** *Oncotarget* (2015) **6**(9):6825-6839.

15. Oltean S, Bates DO: **Hallmarks of alternative splicing in cancer.** *Oncogene* (2014) **33**(46):5311-5318.

16. Wang Y, Chen D, Qian H, Tsai YS, Shao S, Liu Q, Dominguez D, Wang Z: **The splicing factor rbm4 controls apoptosis, proliferation, and migration to suppress tumor progression.** *Cancer Cell* (2014) **26**(3):374-389.

17. Qi Y, Yu J, Han W, Fan X, Qian H, Wei H, Tsai YH, Zhao J, Zhang W, Liu Q, Meng S *et al*: **A splicing isoform of tead4 attenuates the hippo-yap signalling to inhibit tumour proliferation.** *Nat Commun* (2016) **7**(ncomms11840.

18. Cherry S, Lynch KW: **Alternative splicing and cancer: Insights, opportunities, and challenges from an expanding view of the transcriptome.** *Gene Dev* (2020) **34**(15-16):1005-1016.

19. Martinez-Montiel N, Rosas-Murrieta NH, Anaya Ruiz M, Monjaraz-Guzman E, Martinez-Contreras R: **Alternative splicing as a target for cancer treatment.** *International Journal of Molecular Sciences* (2018) **19**(2).

20. Oh J, Pradella D, Kim Y, Shao C, Li H, Choi N, Ha J, Di Matteo A, Fu XD, Zheng X, Ghigna C *et al*: **Global alternative splicing defects in human breast cancer cells.** *Cancers (Basel)* (2021) **13**(12).

21. Storbeck CJ, Wagner S, O'Reilly P, McKay M, Parks RJ, Westphal H, Sabourin LA: **The ldb1 and ldb2 transcriptional cofactors interact with the ste20-like kinase slk and regulate cell migration.** *Mol Biol Cell* (2009) **20**(19):4174-4182.

22. Conway J, Al-Zahrani KN, Pryce BR, Abou-Hamad J, Sabourin LA: **Transforming growth factor beta-induced epithelial to mesenchymal transition requires the ste20-like kinase slk independently of its catalytic activity.** *Oncotarget* (2017) **8**(58):98745-98756.

23. O'Reilly PG, Wagner S, Franks DJ, Cailliau K, Browaeys E, Dissous C, Sabourin LA: **The ste20-like kinase slk is required for cell cycle progression through g2.** *J Biol Chem* (2005) **280**(51):42383-42390.

24. Ellinger-Ziegelbauer H, Karasuyama H, Yamada E, Tsujikawa K, Todokoro K, Nishida E: **Ste20-like kinase (slk), a regulatory kinase for polo-like kinase (plk) during the g2/m transition in somatic cells.** *Genes Cells* (2000) **5**(6):491-498.

25. Cybulsky AV, Takano T, Guillemette J, Papillon J, Volpini RA, Di Battista JA: **The ste20-like kinase slk promotes p53 transactivation and apoptosis.** *Am J Physiol Renal Physiol* (2009) **297**(4):F971-980.

26. Hao W, Takano T, Guillemette J, Papillon J, Ren G, Cybulsky AV: **Induction of apoptosis by the ste20-like kinase slk, a germinal center kinase that activates apoptosis signal-regulating kinase and p38.** *J Biol Chem* (2006) **281**(6):3075-3084.

27. Roovers K, Wagner S, Storbeck CJ, O'Reilly P, Lo V, Northey JJ, Chmielecki J, Muller WJ, Siegel PM, Sabourin LA: **The ste20-like kinase slk is required for erbb2-driven breast cancer cell motility.** *Oncogene* (2009) **28**(31):2839-2848.

28. Johnson TM, Antrobus R, Johnson LN: **Plk1 activation by ste20-like kinase (slk) phosphorylation and polo-box phosphopeptide binding assayed with the substrate translationally controlled tumor protein (tctp).** *Biochemistry* (2008) **47**(12):3688-3696.

29. Tunyasuvunakool K, Adler J, Wu Z, Green T, Zielinski M, Zidek A, Bridgland A, Cowie A, Meyer C, Laydon A, Velankar S *et al*: **Highly accurate protein structure prediction for the human proteome.** *Nature* (2021) **596**(7873):590-596.

30. Consortium GT: **The gtex consortium atlas of genetic regulatory effects across human tissues.** *Science* (2020) **369**(6509):1318-1330.

31. Consortium EP: **An integrated encyclopedia of DNA elements in the human genome.** *Nature* (2012) **489**(7414):57-74.

32. Choi S, Sa M, Cho N, Kim KK, Park SH: **Rbfox2 dissociation from stress granules suppresses cancer progression.** *Exp Mol Med* (2019) **51**(4):1-12.

33. Braeutigam C, Rago L, Rolke A, Waldmeier L, Christofori G, Winter J: **The rna-binding protein rbfox2: An essential regulator of emt-driven alternative splicing and a mediator of cellular invasion.** *Oncogene* (2014) **33**(9):1082-1092.

34. Venables JP, Brosseau JP, Gadea G, Klinck R, Prinos P, Beaulieu JF, Lapointe E, Durand M, Thibault P, Tremblay K, Rousset F *et al*: **Rbfox2 is an important regulator of mesenchymal tissue-specific splicing in both normal and cancer tissues.** *Molecular and Cellular Biology* (2013) **33**(2):396-405.

35. Huh GS, Hynes RO: **Regulation of alternative pre-mrna splicing by a novel repeated hexanucleotide element.** *Genes Dev* (1994) **8**(13):1561-1574.

36. Baron KD, Al-Zahrani K, Conway J, Labreche C, Storbeck CJ, Visvader JE, Sabourin LA: **Recruitment and activation of slk at the leading edge of migrating cells requires src family kinase activity and the lim-only protein 4.** *Biochim Biophys Acta* (2015) **1853**(7):1683-1692.

37. Machicoane M, de Frutos CA, Fink J, Rocancourt M, Lombardi Y, Garel S, Piel M, Echard A: **Slk-dependent activation of erms controls lgn-numa localization and spindle orientation.** *J Cell Biol* (2014) **205**(6):791-799.

38. Quizi JL, Baron K, Al-Zahrani KN, O'Reilly P, Sriram RK, Conway J, Laurin AA, Sabourin LA: **Slk-mediated phosphorylation of paxillin is required for focal adhesion turnover and cell migration.** *Oncogene* (2013) **32**(39):4656-4663.

39. Nowak E, Bednarek I: **Aspects of the epigenetic regulation of emt related to cancer metastasis.** *Cells* (2021) **10**(12).

40. Arnouk H, Yum G, Shah D: **Cripto-1 as a key factor in tumor progression, epithelial to mesenchymal transition and cancer stem cells.** *Int J Mol Sci* (2021) **22**(17).

41. Morcos PA: **Achieving targeted and quantifiable alteration of mrna splicing with morpholino oligos.** *Biochem Biophys Res Commun* (2007) **358**(2):521-527.

42. Pan Q, Shai O, Lee LJ, Frey BJ, Blencowe BJ: **Deep surveying of alternative splicing complexity in the human transcriptome by high-throughput sequencing.** *Nat Genet* (2008) **40**(12):1413-1415.

43. Ying Y, Wang XJ, Vuong CK, Lin CH, Damianov A, Black DL: **Splicing activation by rbfox requires self-aggregation through its tyrosine-rich domain.** *Cell* (2017) **170**(2):312-323 e310.

44. Damianov A, Ying Y, Lin CH, Lee JA, Tran D, Vashisht AA, Bahrami-Samani E, Xing Y, Martin KC, Wohlschlegel JA, Black DL: **Rbfox proteins regulate splicing as part of a large multiprotein complex lasr.** *Cell* (2016) **165**(3):606-619.

45. Blasig IE, Bellmann C, Cording J, Del Vecchio G, Zwanziger D, Huber O, Haseloff RF: **Occludin protein family: Oxidative stress and reducing conditions.** *Antioxid Redox Signal* (2011) **15**(5):1195-1219.

46. Zhong B, Su X, Wen M, Zuo S, Hong L, Lin J: **Parafold: Paralleling alphafold for large-scale predictions.** Abs 1-9.

Acknowledgments

We thank Prof. Yongbo Wang of Fudan University and Prof. Yang Wang of Dalian Medical University for manuscript revision. We thank Ms. Yun Jiang, Dr. Yujie Chen, Ms. Nianhao Cheng, and Ms. Shuang Han for their assistance with the experiments. We are grateful for the experimental support of the UliSchwarz Quantitative Biology Core Facility in Bio-Med Big Data Center, PICB, SINH, CAS. This work is supported by the National Natural Science Foundation of China (32171294) and Shanghai Municipal Natural Science Foundation (20ZR1467300) to H-H.W.. It is also supported by the National Natural Science Foundation of China (31730110, 91940303, and 32030064), the National Key Research and Development Program of China (MOST grant 2018YFA0107602), and the Strategic Priority Research Program of Chinese Academy of Sciences (XDB38040100) to Z.W..

Author contributions:

H-H.W. and Z.W. conceived the project. H-H.W. , Y-Q.Y. and Jing Sun carried out all the molecular and biochemical experiments. W-J.Z. and Y.S. are resiponsible for animal experiments. S-R.Z. and Y.H. analyzed the eCLIP-seq, TCGA data, and performed other bioinformatic analysis. J-F. L and J-W. G. performed protein structure prediction. Y-Q.Y., S-R.Z., Y. H., Y.Y., Z.W. and H-H.W. were responsible for the study design and interpretation of data. All authors were involved in drafting the manuscript and revising it critically for important intellectual content.

Conflict of interest

The authors declare that they have no conflict of interest.

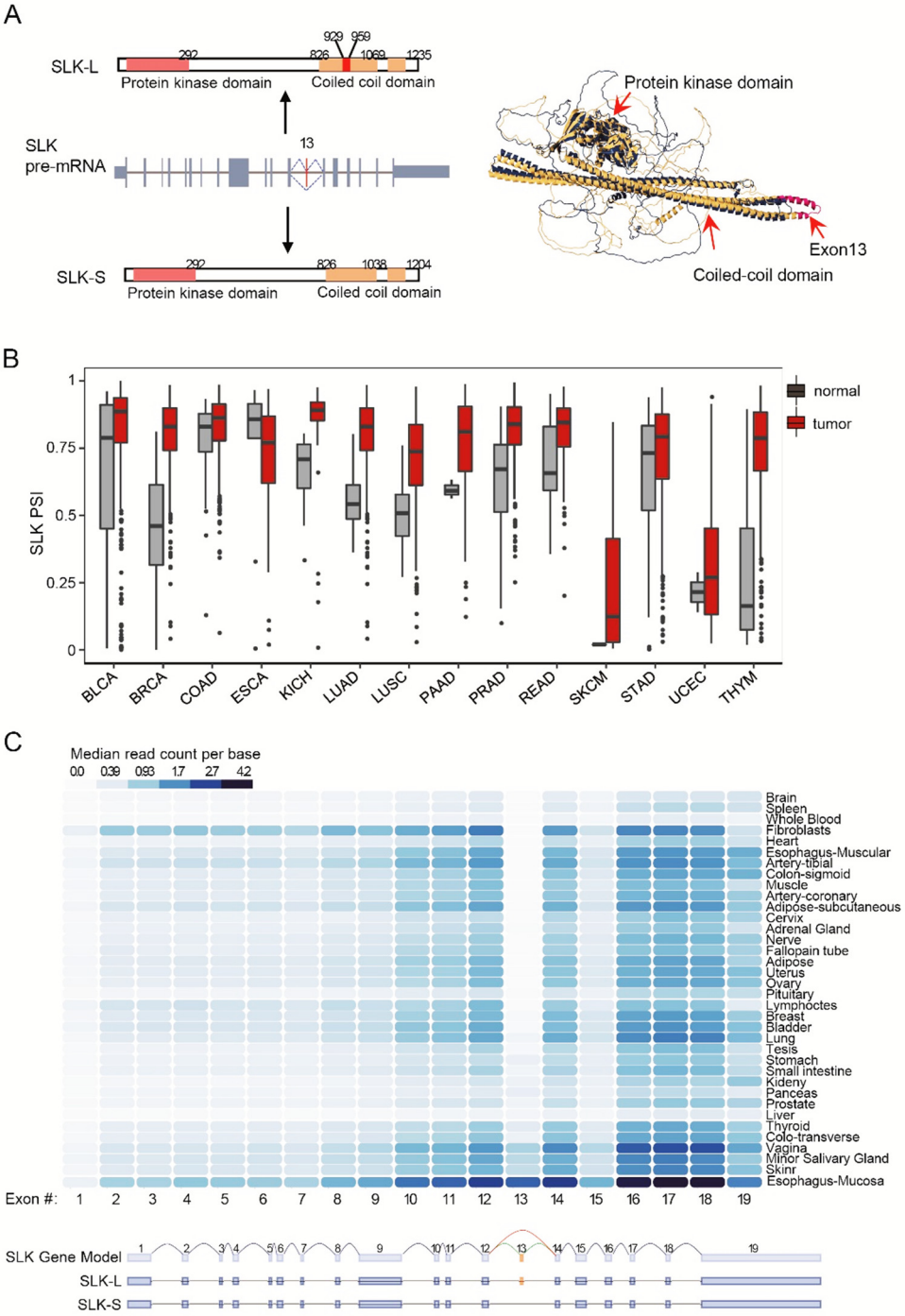

Figure 1 The alternative splicing of SLK alters dramatically in multiple types of human cancer. **A.** Left, schematics of human SLK pre-mRNA and protein. SLK-L included the 13th exon, while SLK-S skipped the 13th exon. Right, The comparison of predicted structure of SLK-L (yellow) and SLK-S isoform (blue). The alternative spliced exon 13th is highlighted in red. **B.** The SLK splicing ratios across various cancer types in TCGA database. PSI: percent spliced in. **C** The expression of SLK isoforms in multiple tissues.

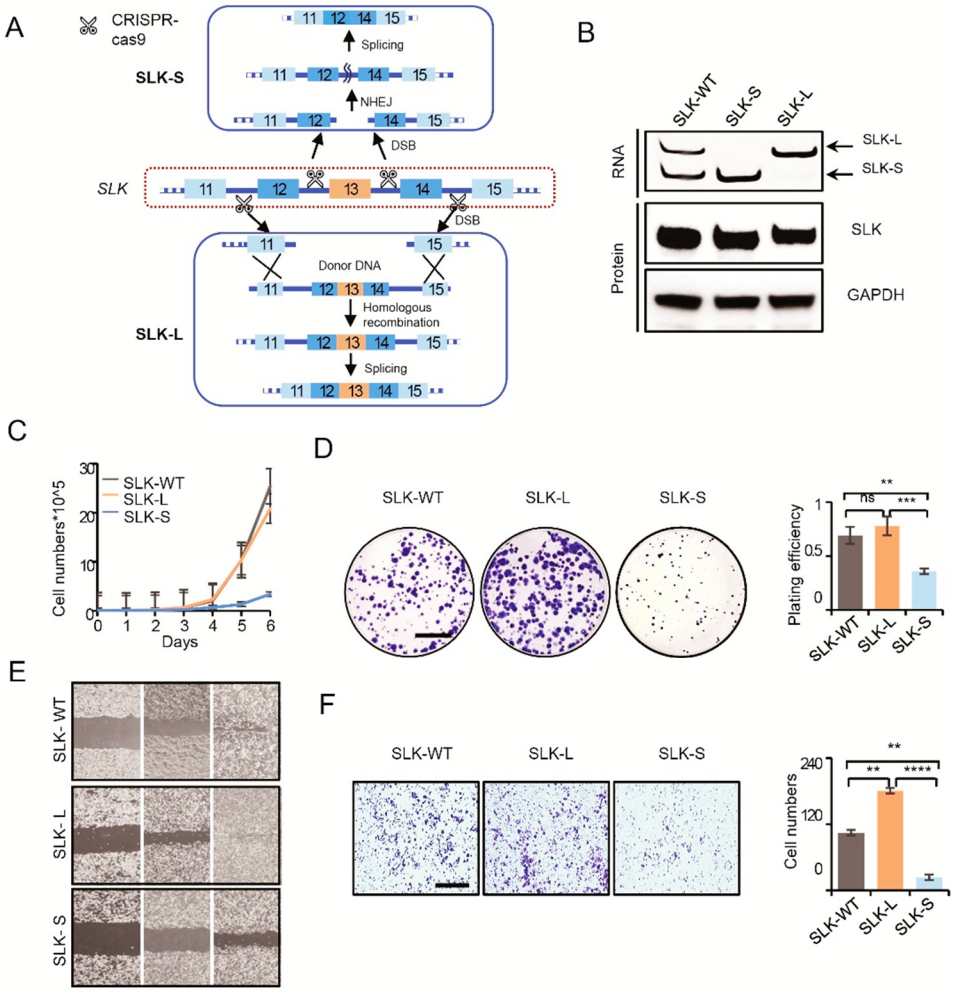

Figure 2 The cancer cells stably express SLK isoforms were generated by CRISPR-cas and exhibited different proliferation and metastasis abilities.**A.** HCT116 cells expressing different SLK isoforms were constructed by CRISPR. **B.** The RNA and protein levels of SLK under gRNA mediated CRISPR genome editing. **C-F.** Cancer cell progression was measured from triplicate experiments, with p values calculated by one-way ANOVA and Tukey's test. **C.** various SLK cells were grown for 6 days, with cell numbers counted every day (n=3) to measure cell growth **D.** anchorage-dependent colony formation of different SLK cell lines (n=3; scale bar:1 cm). The planting efficiency was quantified with ImageJ. **E.** *in vitro* migration of different SLK cell lines was analyzed by wound healing assay (n=3). **F.** cell invasion was measured by transwell assay (n=3; scale bar: 200 μm). Cell number was quantified with ImageJ. *P<0.05, **P<0.01, ***P<0.001, ****P<0.0001, ns, not significant. The chart represents mean±SD.

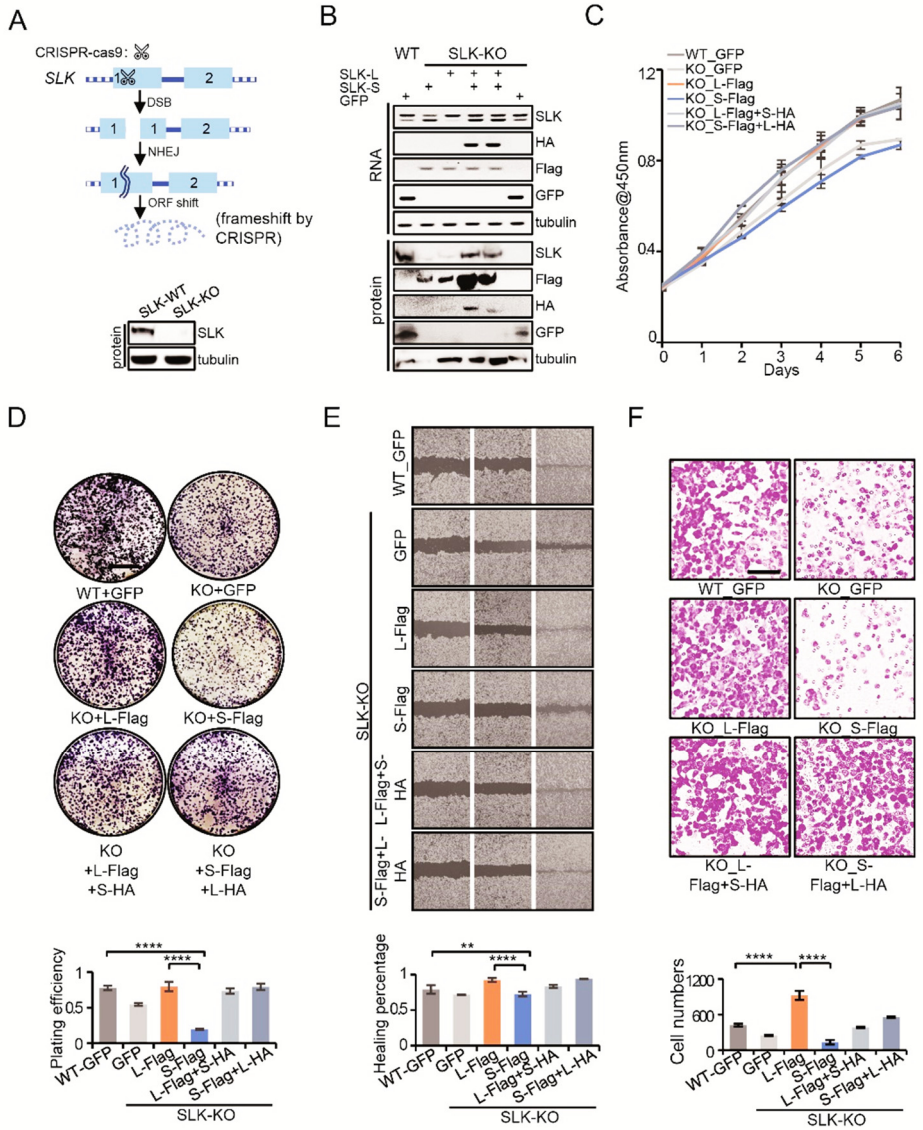

Figure 3 Cancer progression was restored by recovering the expression of the SLK isoforms.**A.** Construction of SLK knockout cell line by CRISPR. **B.** SLK isoforms were re-expressed in SLK knockout cells, with the RNA and protein level of SLK detected accordingly. **C-F.** Cancer cell development was measured as described in Fig. 2.

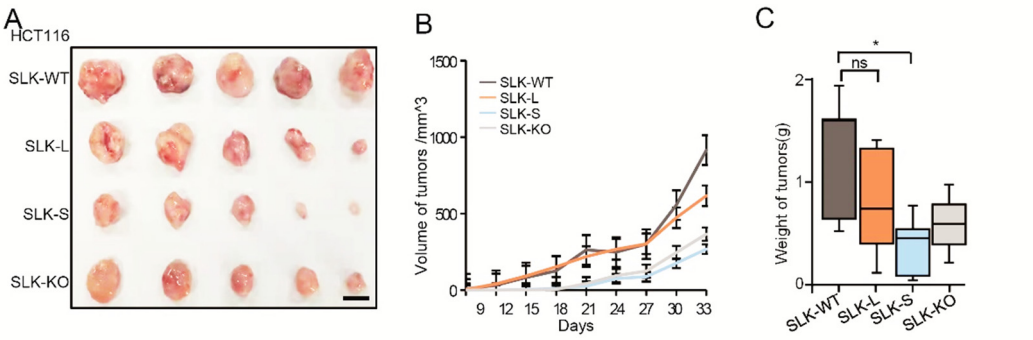

Figure 4 The deficiency of SLK long isoform inhibits tumor growth in xenograft mice. **A** Xenograft tumors were generated using nude mice injected with SLK-WT, SLK-L, SLK-S, or SLK-KO cells (1×10^6 cells/mouse), respectively. **B.** Tumors were removed after five weeks, and tumor volume was quantified (n=5). **C** The weight of xenograft tumors were plotted as box plot. The chart represents mean±SD. *P<0.05, ns, not significant. Dunnett's test was used in B and C.

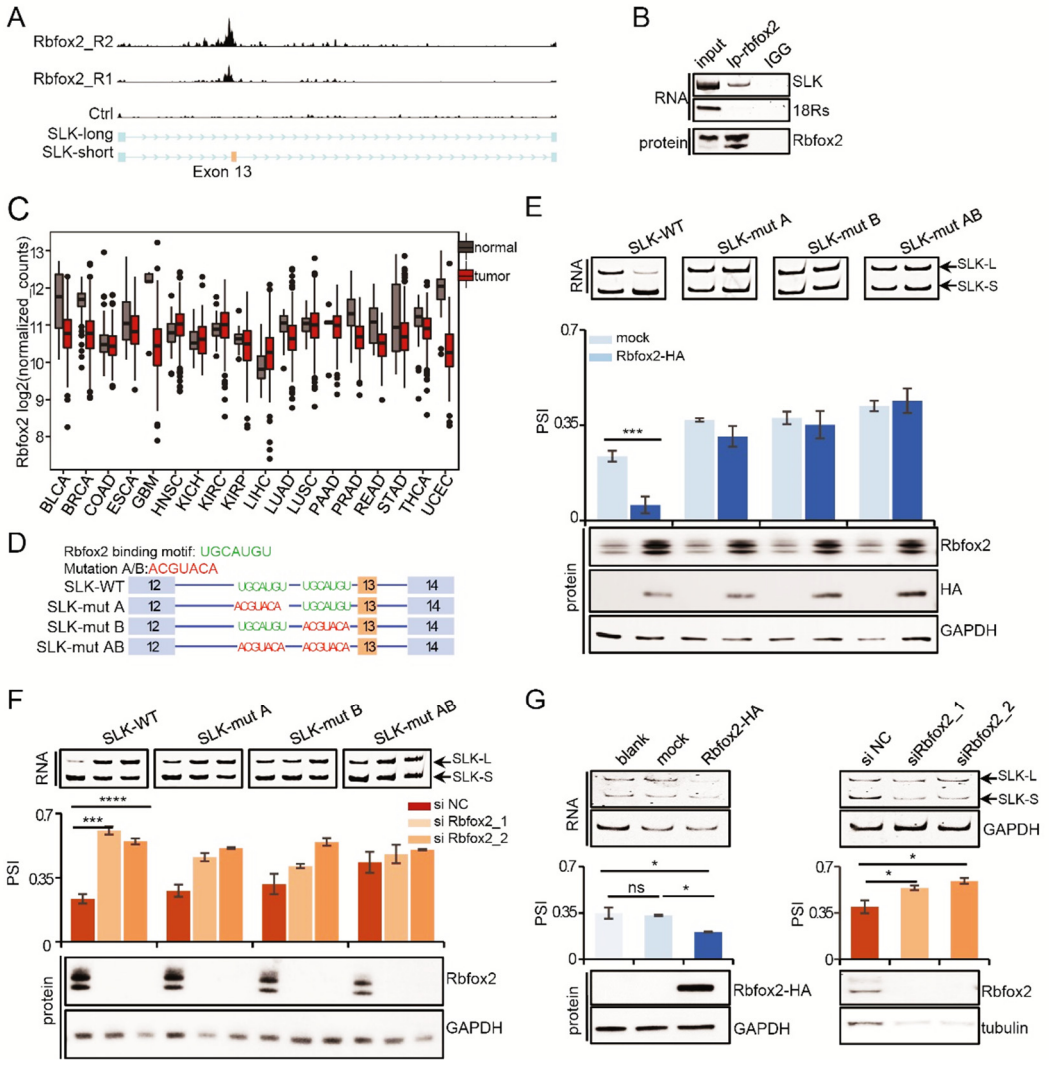

Figure 5 Rbfox2 regulates the splicing of SLK. **A.** Rbfox2 binding peaks was detected in front of the SLK exon 13th. **B.** The RIP assay showed the binding of Rbfox2 to SLK RNA. **C.** Rbfox2 expression level in tumors versus normal tissues across various cancer types from TCGA data. **D.** The minigene reporter of SLK wildtype and mutants were constructed. **E-G.** Rbfox2 regulates SLK splicing through its binding motif. **E.** Rbfox2 overexpression inhibited SLK minigene splicing. **F.** Rbfox2 knockdown promoted SLK minigene splicing. **G**. Rbfox2 regulates splicing of the endogenous *SLK* gene. RNA loading control: GAPDH; protein loading control: GAPDH or Tubulin. The chart represents mean±SD. *P<0.05, **P<0.01, ***P<0.001, ****P<0.0001. Two-way ANOVA was applied to analyze the difference among means in E and F while one-way ANOVA was used in G.

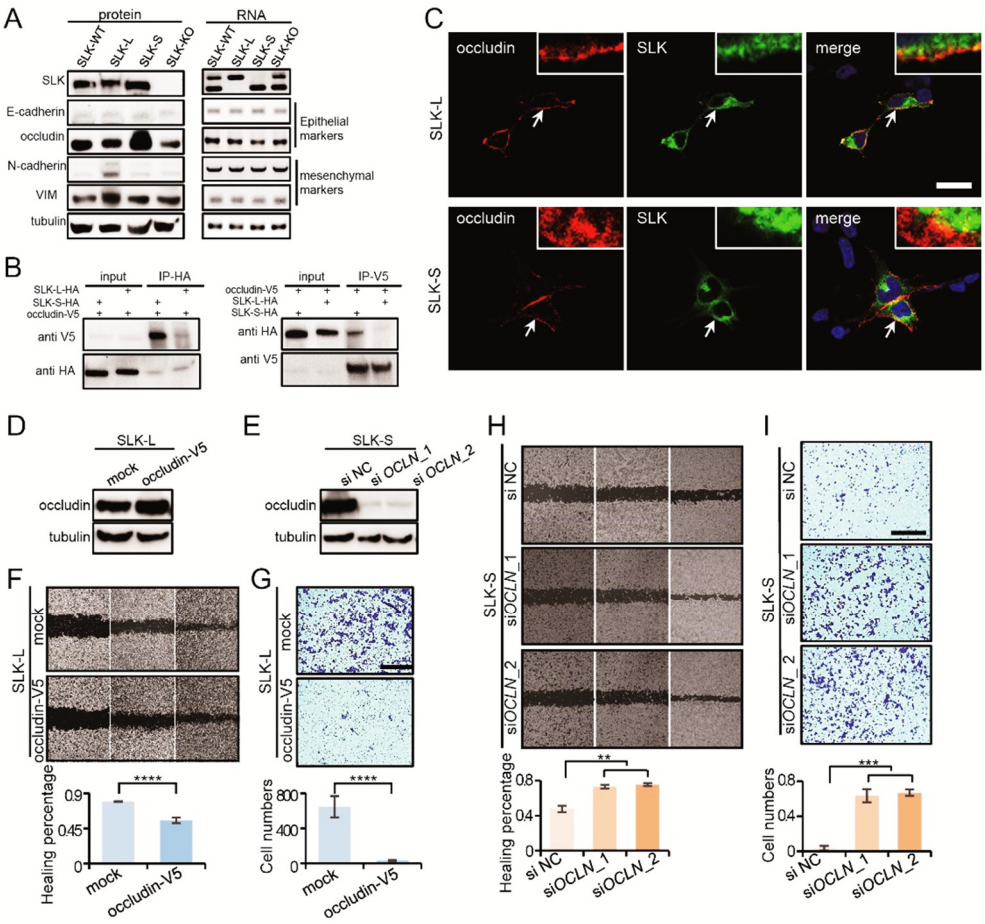

Figure 6 SLK isoforms influence cell functions partially through their different binding abilities to occludin. **A.** Selected EMT markers were tested in different SLK cell lines. **B.** SLK isoforms showed varied binding abilities with occludin. **C.** The subcellular localization of SLK and Occludin. Scale bar: 20 μm. **D-E.** Overexpression or knockdown of occlidin in SLK-L or SLK-S cells. **F-I.** Cell migration (n=3) and invasion (n=3; scale bar:200 μm) were tested as described in Fig. 2. *P<0.05, **P<0.01, ***P<0.001, ****P<0.0001.

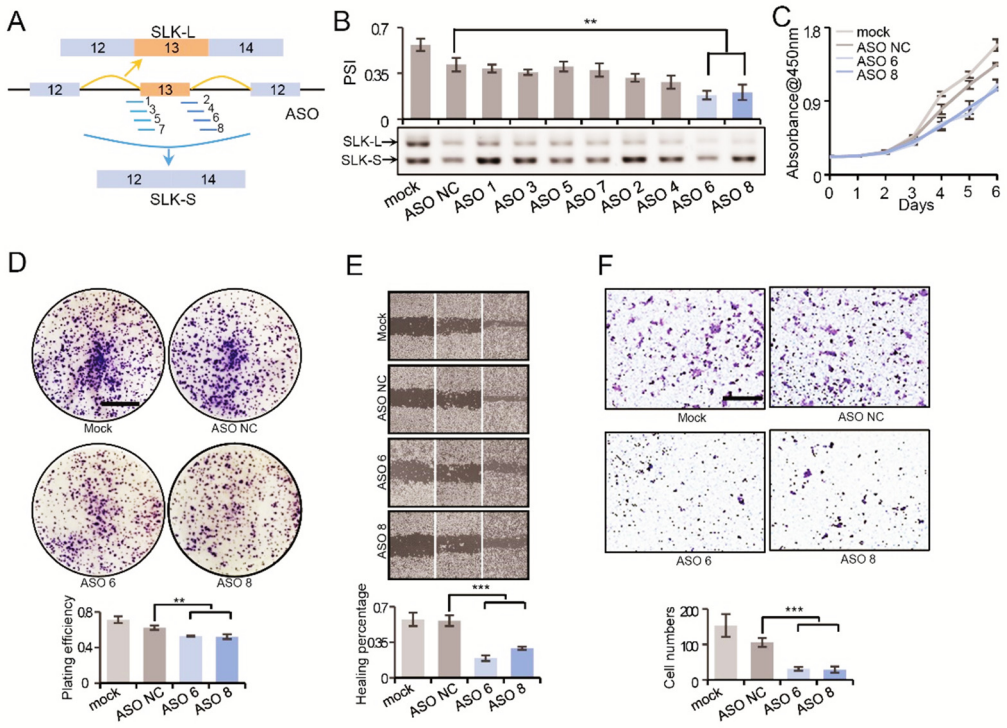

Figure 7 ASOs affected cancer progression by regulating SLK splicing. **A** The Design of ASOs that specifically block SLK splicing. **B** The PSI of SLK splicing in cells treated with indicated ASOs. **C-F** Cellular proliferation rates (C; n=3), colony formation (D; n=3; scale bar: 1 cm); migration (E; n=3), and invasion (F; n=3; scale bar: 200 μm) were tested according to Fig. 2 *P<0.05, **P<0.01, ***P<0.001, ****P<0.0001, ns, not significant.